

ERQA: Edge-Restoration Quality Assessment for Video Super-Resolution

Anastasia Kirillova¹^a, Eugene Lyapustin¹^b, Anastasia Antsiferova¹^c and Dmitry Vatolin¹^d

¹*Lomonosov Moscow State University, Moscow, Russia*

{*anastasia.kirillova, evgeny.lyapustin, aantsiferova, dmitriy*}@graphics.cs.msu.ru

Keywords: Video Super-Resolution, Quality Assessment, Video Restoration

Abstract: Despite the growing popularity of video super-resolution (VSR), there is still no good way to assess the quality of the restored details in upscaled frames. Some VSR methods may produce the wrong digit or an entirely different face. Whether a method’s results are trustworthy depends on how well it restores truthful details. Image super-resolution can use natural distributions to produce a high-resolution image that is only somewhat similar to the real one. VSR enables exploration of additional information in neighboring frames to restore details from the original scene. The ERQA metric, which we propose in this paper, aims to estimate a model’s ability to restore real details using VSR. On the assumption that edges are significant for detail and character recognition, we chose edge fidelity as the foundation for this metric. Experimental validation of our work is based on the MSU Video Super-Resolution Benchmark, which includes the most difficult patterns for detail restoration and verifies the fidelity of details from the original frame. Code for the proposed metric is publicly available at <https://github.com/msu-video-group/ERQA>.

1 INTRODUCTION

As a fundamental image- and video-processing task, super-resolution remains a popular research topic. It has a wide range of applications, from low-complexity encoding¹ to old-film restoration and medical-image enhancement. Trends in quality assessment of upscaled videos and images are favoring estimation of statistical naturalness in combination with fidelity. But restoration fidelity is much more important than statistical naturalness for some tasks: small-object recognition (e.g., license-plate numbers) in CCTV recordings, text recognition, and medical-image reconstruction.

With the development of deep-learning-based approaches, many super-resolution models produce visually natural frames but lose important details. For example, the rightmost image in Figure 2, upscaled by TDAN (Tian et al., 2020), is perceptually better than the leftmost one, upscaled by RRN-10L (Isobe et al., 2020), but the shape of the shiny thread in the left-

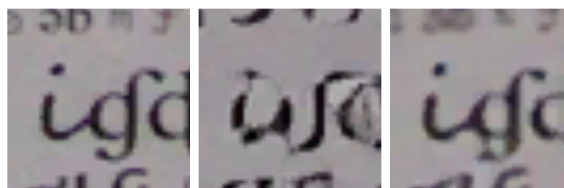




Figure 1: Example of changing context in an upscaled video: two characters from source frame (GT, leftmost) mix to yield a new one during video upsampling.





Figure 2: Example of upscaled images that vary in detail-restoration quality. The rightmost image is visually more natural, but the shape of the details in the leftmost image is closer to the original.

most image is closer to ground truth (GT, center). Occasionally, such models can even change the context in an image by, for example, producing an incorrect number, character, or even human face without decreasing traditional-metric values. In Figure 1, Real-ESRGAN (Wang et al., 2021) mixed two letters from low-resolution images to form a completely different

^a <https://orcid.org/0000-0002-0799-3135>

^b <https://orcid.org/0000-0002-2515-9478>

^c <https://orcid.org/0000-0002-1272-5135>

^d <https://orcid.org/0000-0002-8893-9340>

¹<https://www.lcevc.org/>

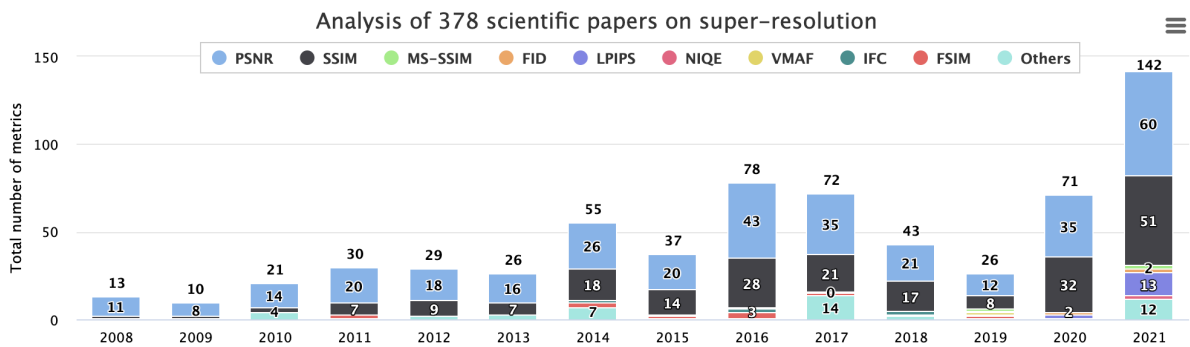


Figure 3: Metrics for estimating super-resolution quality cited in papers proposing new methods, by year. PSNR and SSIM (Wang et al., 2004) are the most popular; LPIPS (Zhang et al., 2018) saw wide use in 2020 and 2021.

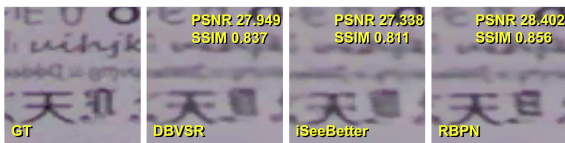


Figure 4: Example of changing context in an upscaled video: RBPN (Haris et al., 2019) has changed a character in the rightmost image.



Figure 5: Example of changing context in an upscaled video: unnatural faces are the result here, differing considerably from the source one (GT, leftmost).

letter (center). In Figure 4, RBPN (Haris et al., 2019) added horizontal lines to the bottom-right character, but all three models score the same on traditional metrics. In Figure 5, Real-ESRGAN (Wang et al., 2021) and RealSR (Ji et al., 2020) produced unnatural faces that greatly differ from the source one.

The examples in Figures 1–2, 4–5 demonstrate that assessment of detail-restoration quality for image and video super-resolution is difficult. The best way to estimate restoration fidelity is to conduct a subjective comparison; it’s the most precise approach but is time consuming and expensive. Another way involves reference quality metrics. Traditional similarity metrics such as PSNR and SSIM (Wang et al., 2004) are often used to evaluate super-resolution models, but they yield poor results and are unstable when dealing with shifts and other common super-resolution artifacts. LPIPS (Zhang et al., 2018) is increasingly popular for this task, but it originally aimed to assess perceptual similarity rather than fidelity. The new DISTS (Ding et al., 2020a) metric is an improvement on LPIPS, but it also focuses on perceptual similarity.

Our research focuses on analyzing super-

resolution algorithms, particularly their restoration fidelity. When we started working on a benchmark for video super-resolution², including a test for restoration-quality assessment, we discovered that existing metrics work fine for other tests (restoration naturalness and beauty) but have a low correlation with subjective detail-quality estimation. In this paper, therefore, we introduce a new method for evaluating information fidelity. Experiments reveal that our metric outperforms other super-resolution quality metrics in assessing detail restoration.

The main contributions of our work are the following:

1. A video-super-resolution benchmark based on a new dataset containing the most difficult patterns for detail restoration.
2. A subjective comparison examining the fidelity of details from the original frame, instead of traditional statistical naturalness and beauty.
3. A new metric for assessing the detail-restoration quality of video super-resolution.

2 RELATED WORK

PSNR and SSIM (Wang et al., 2004) are common metrics for assessing super-resolution quality. We analyzed 378 papers that propose super-resolution methods and found that since 2008, PSNR and SSIM have remained the most popular metrics. But both have been shown to exhibit a low correlation with subjective scores. LPIPS (Zhang et al., 2018) has grown in popularity over the last two years; other metrics remain less popular (Figure 3).

Several full-reference metrics for assessing super-resolution visual quality have emerged. (Wan et al.,

²<https://videoprocessing.ai/benchmarks/video-super-resolution.html>

Table 1: A comparison of datasets using for testing super-resolution quality assessment approaches.

Dataset	# references	# SR images	# SR algorithms	Subjective type
C. Ma et al.’s (Ma et al., 2017)	30	1620	9	MOS
QADS (Zhou et al., 2019)	20	980	21	Pairwise comparison
SupER (Köhler et al., 2019)	14	3024	20	Pairwise comparison
SRIJ (Beron et al., 2020)	32	608	7	MOS
SISRSet (Shi et al., 2019)	15	360	8	MOS
ECCV (Yang et al., 2014)	10	540	6	MOS
SRID (Wang et al., 2017)	20	480	8	MOS

2018) used four features (gradient magnitude, phase congruency, anisotropy, and directionality complexity) to calculate the perceptual structure measurement (PFSM) in both the upscaled and original high-resolution frames. Similarity function applied to PFSMs showed more-consistent results than previous approaches with regard to visual perception on their dataset. (Zhou et al., 2021) calculated structural fidelity and statistical naturalness, fused these coefficients into a weighted sum, and achieved good correlation on the QADS image database (Zhou et al., 2019).

Another popular approach is to extract structure or texture features from LR and upscaled (SR) images, compare them separately, and fuse the resulting similarity indices (Yeganeh et al., 2015; Fang et al., 2019). Metrics based on this idea achieve a Spearman rank correlation coefficient (SRCC) coefficient of 0.69 to 0.85 on various datasets. (Yang et al., 2019) trained a regression model using statistical features extracted from LR and SR images, obtaining a correlation similar to that of other top metrics on the dataset from (Ma et al., 2017). (Shi et al., 2019) proposed another approach for reduced-reference assessment that uses the visual-content-prediction model to measure the structure of the reference and SR images. This method outperforms previous ones on the SISRSSet dataset (Shi et al., 2019).

A number of no-reference metrics are also used for video super-resolution. (Ma et al., 2017) trains regression models on statistical features extracted from upscaled frames, achieving high value of SRCC on their dataset. (Zhang et al., 2021) proposed a no-reference metric, based on features extracted using a pretrained neural network—VGGNet. (Wang et al., 2018) trained SVM using extracted features and obtained results similar to those of other metrics. (Greeshma and Bindu, 2020) proposed the SRQC metric, which estimates structure changes and quality-aware features. This metric exhibits good results, but they consider only a few images and four SR methods for the test dataset.

Edges have a strong influence on the human vi-

sual system. Furthermore, edge fidelity is a base criterion for assessing detail-restoration quality. Several methods thus consider edge features as the basis for quality assessment. Some calculate edge features, including number, length, direction, strength, contrast, and width, and compare them using the similarity measure to estimate image or video quality (Attar et al., 2016; Ni et al., 2017). Nevertheless, these metrics achieve on their datasets almost the same correlation as traditional PSNR and SSIM. In (Xue and Mou, 2011), the authors detected edges in both reference and distorted images and compared them by calculating recall. (Chen et al., 2011) used histogram analysis for edge comparison. These metrics deliver a slightly greater correlation than PSNR and SSIM. Liu et al. (Liu et al., 2019) proposed using the F1 score to evaluate edge fidelity, but they declined to conduct a comparison with other metrics and kept their code under wraps. Our method is based on the same edge-comparison idea, but it’s robust for small local and global edge shifts, which appear during super-resolution but are unessential for detail recognition. It yielded much better results than other quality-assessment approaches.

A number of datasets are used for testing super-resolution quality assessment (Table 1), but not for detail restoration, because they lack difficult patterns for that task as in Figure 6 (text, numbers, QR codes, faces, complex textures). Therefore, we built a dataset for assessing super-resolution quality that includes the most challenging content for detail restoration.

Summarizing the above analysis, few metrics aim to assess and compare detail-restoration quality. Some that use edge features have emerged, but no one uses them for super-resolution, which involves peculiar artifacts. Therefore, it’s important to obtain an objective metric that correlates highly with human estimation of detail-restoration quality and that allows comparison of super-resolution models, not only for naturalness but also for information fidelity.

3 PROPOSED METHOD

3.1 Dataset

To analyze a VSR model’s ability to restore real details, we built a test stand containing patterns that are difficult for video restoration (Figure 6).

To calculate metrics for particular content types and to verify how a model works with different inputs, we divide each output frame into parts by detecting crosses:

- Part 1 “Board” includes a few small objects and photos of human faces³. Our goal is to obtain results for the model operating on textures with small details. The striped fabric and balls of yarn may produce a Moire pattern (Figure 7). Restoration of human faces is important for video surveillance.
- Part 2 “QR” comprises multiple QR codes of differing sizes; the aim is to find the size of the smallest recognizable one in the model’s output frame. A low-resolution frame may blend QR-code patterns, so models may have difficulty restoring them.
- Part 3 “Text” includes two kinds: handwritten and typed. Packing all these difficult elements into the training dataset is a challenge, so they are each new to the model as it attempts to restore them.
- Part 4 “Metal paper” contains foil that was vigorously crumpled. It’s an interesting example because of the reflections, which change periodically between frames.
- Part 5 “Color lines” is a printed image with numerous thin color stripes. This image is difficult because thin lines of similar colors end up mixing in low-resolution frames.
- Part 6 “License-plate numbers” consists of a set of car license plates of varying sizes from different countries⁴. This content is important for video surveillance and dashcam development.
- Part 7 “Noise” includes difficult noise patterns. Models cannot restore real ground-truth noise, and each one produces a unique pattern.
- Part 8 “Mira” contains a resolution test chart with patterns that are difficult to restore: a set of straight and curved lines of differing thicknesses and directions.

³Photos were generated by <https://thispersondoesnotexist.com/>

⁴The license-plate numbers are generated randomly and printed on paper.

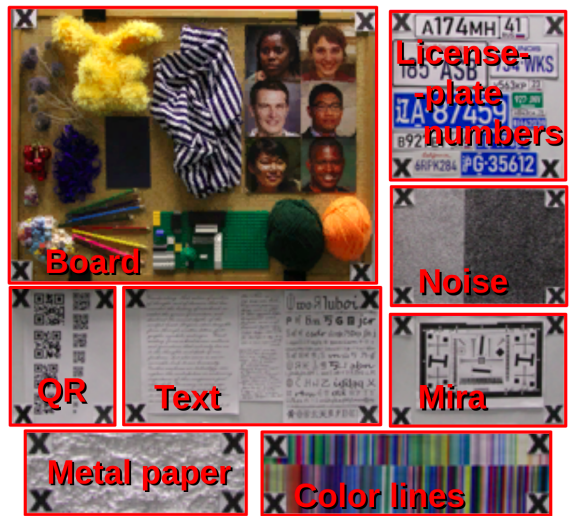


Figure 6: Test stand for the proposed VSR benchmark. The size of the stand $3,456 \times 3,456$ pixels in a source video and $1,280 \times 1,280$ pixels in a ground truth video.



Figure 7: Example of a Moire pattern on the “Board.” There is a zoomed result on the right.

We captured the dataset using a Canon EOS 7D camera. We quickly took a series of 100 photos and used them as a video sequence. The shots were from a fixed point without a tripod, so the video contains a small amount of random motion. We stored the video as a sequence of frames in PNG format, converted from JPG. The camera’s settings were ISO 4000, aperture 400, and resolution 5184×3456 .

The source video also has a resolution of 5184×3456 and was stored in the sRGB color space. We degraded it using bicubic interpolation to generate a ground truth of resolution 1920×1280 . This step is essential because many open-source models lack the code to process a large frame; processing large frames is also time consuming. We further degraded the input video from ground truth, again using bicubic interpolation, to 480×320 to test the models for $4\times$ upscaling. The output of each model is also a sequence of frames, which we compare with the ground-truth sequence to verify the model’s performance.

3.2 Subjective Comparison

We used 21 super-resolution algorithms in our quality assessment. We also added a ground-truth video, so

the experimental validation involves 22 videos. We cut the sequences to 30 frames and converted them to 8 frames per second (fps). This length allows subjects to easily consider details and decide which video is better. We then cropped from each video 10 snippets that cover the most difficult patterns for restoration and conducted a side-by-side pairwise subjective evaluation using the Subjectify.us service, which enables crowd-sourced comparisons.

To estimate information fidelity, we asked participants in the subjective comparison to avoid choosing the most beautiful video, but instead choose the one that shows better detail restoration. Participants are not experts in this field thus they do not have professional biases. Each participant was shown 25 paired videos and in each case had to choose the best video (“indistinguishable” was also an option). Each pair of snippets was shown to 10-15 participants until confidence interval stops changing. Three of pairs for each participant are for verification, so the final results exclude their answers. All other responses from 1400 successful participants are used to predict subjective scores using the Bradley-Terry (Bradley and Terry, 1952).

3.3 Edge Restoration Quality Assessment Method

On the basis of the hypothesis that edges are significant for detail restoration, we developed the edge-restoration quality assessment (ERQA) metric, which estimates how well a model can restore edges in a high-resolution frame. Our metric compensates for small global and local edge shifts, assuming they don’t complicate detail recognition.

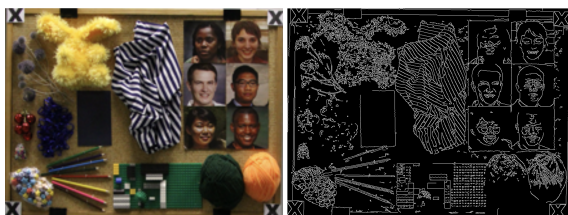


Figure 8: The content part “Board” cropped from a GT frame (left) along with edges of this frame highlighted with the Canny algorithm (Canny, 1986) with chosen parameters (right).

First, we find edges in both the output and ground-truth frames. Our approach uses an OpenCV implementation⁵ of the Canny algorithm (Canny, 1986). The threshold for initially identifying strong edges is 200, and the threshold for linking edges is 100. These

⁵https://docs.opencv.org/3.4/dd/d1a/group_imgproc__feature.html#ga04723e007ed888ddf11d9ba04e2232de



Figure 9: Crop from an upscaled frame (left), crop from the source frame (right) and visualization of ERQA metric (center). White = true positive, blue = false negative, red = false positive.

coefficients allow us to highlight the edges of all objects, even small ones, while skipping lines, which are unimportant (Figure 8).

Having found the edges in the ground-truth and distorted frames as binary masks, we compare them using the F1 score:

$$precision = \frac{TP}{TP + FP}, recall = \frac{TP}{TP + FN}, \quad (1)$$

$$F_1 = 2 \frac{precision \cdot recall}{precision + recall}, \quad (2)$$

where TP (True Positive) is a number of pixels detected as edge in both ground-truth and distorted frames, FP (False Positive) is a number of pixels detected as edges only in distorted frame, FN (False Negative) is a number of pixels detected as edges only in ground-truth frame (Figure 9).

Some models can generate frames with a global pixel shift relative to ground truth, so we checked the integer pixel shifts $[-3, 3]$ along both axes and chose the one with the maximum PSNR value. Compensating for this global shift aids our metric considerably (Table 4).

During an upscaling, models may also shift edge pixels locally, which in many cases is insignificant to human perception of information. To compensate for local single-pixel edge shifts, we consider as true positive any pixels on the output edges, which are not on the ground-truth edges but are near (on the difference of one pixel) with the edge of GT.

We then noticed that some models produce a wider edge compared with the ground truth, and our method with local compensation (ERQAv1.0) marks these edges as fully true positive. To correct this shortcoming, ERQAv1.1 considers each point on a ground-truth edge as corresponding to true positive only once. The overall pipeline of Edge Restoration Quality Assessment method:

Table 2: Spearman rank correlation coefficient (SRCC) of metrics with subjective assessment on all test cases. Metrics calculated on each test case compared with subjective score on the same test case. Mean value of correlation coefficients is also presented.

Metric	Lego	Toy	Faces	Yarn	QRs	Text-1	Text-2	Car-1	Car-2	Mira	Mean
ERQAv1.0	0.87	0.72	0.85	0.85	0.66	0.85	0.89	0.86	0.79	0.38	0.77
ERQAv1.1	0.87	0.66	0.89	0.84	0.65	0.85	0.91	0.92	0.88	0.41	0.79
SSIM*	0.68	0.20	0.81	0.33	0.52	0.57	0.63	0.86	0.86	0.29	0.58
PSNR*	0.36	-0.05	0.66	0.14	0.40	0.40	0.54	0.82	0.72	0.06	0.41
LPIPS	0.70	0.79	0.52	0.79	0.68	0.88	0.63	0.67	0.67	0.75	0.71
LPIPS*	0.78	0.81	0.56	0.84	0.69	0.88	0.65	0.72	0.71	0.75	0.74
DISTS	0.6	0.35	0.69	0.65	0.54	0.84	0.79	0.74	0.72	0.58	0.65
DISTS*	0.6	0.35	0.72	0.71	0.58	0.86	0.88	0.87	0.81	0.56	0.694
MS-SSIM	0.38	0.30	0.59	0.20	0.32	0.48	0.47	0.56	0.59	0.39	0.43
MS-SSIM*	0.77	0.19	0.68	0.35	0.48	0.53	0.6	0.82	0.81	0.25	0.55
VMAF	0.36	0.35	0.61	0.33	0.36	0.52	0.53	0.55	0.60	0.48	0.47
VMAF*	0.33	0.36	0.57	0.38	0.34	0.52	0.48	0.56	0.58	0.47	0.46
VMAF (clip)	0.36	0.35	0.60	0.33	0.36	0.52	0.53	0.55	0.59	0.49	0.47
VMAF (clip)*	0.33	0.36	0.56	0.38	0.34	0.52	0.48	0.56	0.57	0.47	0.46
Ma et al.	0.47	0.88	-0.28	0.62	0.71	—	—	—	—	—	0.48

Table 3: Performance comparison of all metrics with and without global compensation shifts.

Metric	Without compensation		With global pixel shift compensation	
	PLCC	SRCC	PLCC	SRCC
LPIPS	0.8103	0.7077	0.8352 (+0.0249)	0.7377 (+0.0300)
DISTS	0.8094	0.6513	0.8278 (+0.0184)	0.6931 (+0.0418)
MS-SSIM	0.2796	0.4282	0.5992 (+0.3196)	0.5484 (+0.1202)
VMAF	0.2998	0.4692	0.2644 (-0.0354)	0.4572 (-0.012)
VMAF(not clipped)	0.3428	0.4706	0.2999 (-0.0429)	0.4586 (-0.012)

Table 4: An ablation study of the proposed method.

Stage	PLCC	SRCC
Without compensation (baseline)	0.5035	0.4745
+ Compensation of global shift	0.7395 (+0.2360)	0.6342 (+0.1597)
+ Compensation of local shift (v1.0)	0.8243 (+0.0848)	0.7383 (+0.1041)
+ Penalize false wide edges (v1.1)	0.8316 (+0.0540)	0.7519 (+0.0486)

REFERENCES

- Attar, A., Shahbahrami, A., and Rad, R. M. (2016). Image quality assessment using edge based features. *Multimedia Tools and Applications*, 75(12):7407–7422.
- Beron, J., Benitez-Restrepo, H. D., and Bovik, A. C. (2020). Blind image quality assessment for super resolution via optimal feature selection. *IEEE Access*, 8:143201–143218.
- Bradley, R. A. and Terry, M. E. (1952). Rank analysis of incomplete block designs: I. the method of paired comparisons. *Biometrika*, 39(3/4):324–345.
- Canny, J. (1986). A computational approach to edge detection. *IEEE Transactions on Pattern Analysis and Machine Intelligence*, PAMI-8(6):679–698.
- Chen, X., Zhang, R., and Zheng, S. (2011). Image quality assessment based on local edge direction histogram. In *2011 International Conference on Image Analysis and Signal Processing*, pages 108–112. IEEE.
- Ding, K., Ma, K., Wang, S., and Simoncelli, E. P. (2020a). Image quality assessment: Unifying structure and texture similarity. *arXiv preprint arXiv:2004.07728*.
- Ding, K., Ma, K., Wang, S., and Simoncelli, E. P. (2020b). Image quality assessment: Unifying structure and texture similarity. *CoRR*, abs/2004.07728.
- Fang, Y., Liu, J., Zhang, Y., Lin, W., and Guo, Z. (2019). Reduced-reference quality assessment of image super-resolution by energy change and texture variation. *Journal of Visual Communication and Image Representation*, 60:140–148.
- Greeshma, M. and Bindu, V. (2020). Super-resolution quality criterion (srqc): a super-resolution image quality assessment metric. *Multimedia Tools and Applications*, 79(47):35125–35146.
- Haris, M., Shakhnarovich, G., and Ukita, N. (2019). Recurrent back-projection network for video super-resolution. In *Proceedings of the IEEE/CVF Conference on Computer Vision and Pattern Recognition*,

- pages 3897–3906.
- Isobe, T., Zhu, F., Jia, X., and Wang, S. (2020). Revisiting temporal modeling for video super-resolution. *arXiv preprint arXiv:2008.05765*.
- Ji, X., Cao, Y., Tai, Y., Wang, C., Li, J., and Huang, F. (2020). Real-world super-resolution via kernel estimation and noise injection. In *Proceedings of the IEEE/CVF Conference on Computer Vision and Pattern Recognition Workshops*, pages 466–467.
- Köhler, T., Bätz, M., Naderi, F., Kaup, A., Maier, A., and Riess, C. (2019). Toward bridging the simulated-to-real gap: Benchmarking super-resolution on real data. *IEEE transactions on pattern analysis and machine intelligence*, 42(11):2944–2959.
- Liu, S., Peng, X., and Liu, Z. (2019). Image quality assessment through contour detection. In *2019 IEEE 28th International Symposium on Industrial Electronics (ISIE)*, pages 1413–1417. IEEE.
- Ma, C., Yang, C.-Y., Yang, X., and Yang, M.-H. (2017). Learning a no-reference quality metric for single-image super-resolution. *Computer Vision and Image Understanding*, 158:1–16.
- Ni, Z., Ma, L., Zeng, H., Chen, J., Cai, C., and Ma, K.-K. (2017). Esim: Edge similarity for screen content image quality assessment. *IEEE Transactions on Image Processing*, 26(10):4818–4831.
- Prewitt, J. M. (1970). Object enhancement and extraction. *Picture processing and Psychopictorics*, 10(1):15–19.
- Roberts, L. G. (1963). *Machine perception of three-dimensional solids*. PhD thesis, Massachusetts Institute of Technology.
- Shi, G., Wan, W., Wu, J., Xie, X., Dong, W., and Wu, H. R. (2019). Sisrset: Single image super-resolution subjective evaluation test and objective quality assessment. *Neurocomputing*, 360:37–51.
- Tian, Y., Zhang, Y., Fu, Y., and Xu, C. (2020). Tdan: Temporally-deformable alignment network for video super-resolution. In *Proceedings of the IEEE/CVF Conference on Computer Vision and Pattern Recognition*, pages 3360–3369.
- Wan, W., Wu, J., Shi, G., Li, Y., and Dong, W. (2018). Super-resolution quality assessment: Subjective evaluation database and quality index based on perceptual structure measurement. In *2018 IEEE International Conference on Multimedia and Expo (ICME)*, pages 1–6. IEEE.
- Wang, G., Li, L., Li, Q., Gu, K., Lu, Z., and Qian, J. (2017). Perceptual evaluation of single-image super-resolution reconstruction. In *2017 IEEE International Conference on Image Processing (ICIP)*, pages 3145–3149. IEEE.
- Wang, G., Zhu, F., Lu, Z., Yuan, X., and Li, L. (2018). No-reference quality assessment of super-resolution reconstructed images by incorporating domain knowledge. *J. Inf. Hiding Multim. Signal Process.*, 9(2):496–505.
- Wang, X., Xie, L., Dong, C., and Shan, Y. (2021). Real-esrgan: Training real-world blind super-resolution with pure synthetic data. *arXiv preprint arXiv:2107.10833*.
- Wang, Z., Bovik, A. C., Sheikh, H. R., and Simoncelli, E. P. (2004). Image quality assessment: from error visibility to structural similarity. *IEEE transactions on image processing*, 13(4):600–612.
- Wang, Z., Simoncelli, E. P., and Bovik, A. C. (2003). Multiscale structural similarity for image quality assessment. In *The Thirty-Seventh Asilomar Conference on Signals, Systems & Computers, 2003*, volume 2, pages 1398–1402. Ieee.
- Xue, W. and Mou, X. (2011). An image quality assessment metric based on non-shift edge. In *2011 18th IEEE International Conference on Image Processing*, pages 3309–3312. IEEE.
- Yang, C.-Y., Ma, C., and Yang, M.-H. (2014). Single-image super-resolution: A benchmark. In *European conference on computer vision*, pages 372–386. Springer.
- Yang, L., Sheng, Y., and Chai, L. (2019). A machine learning based reduced-reference image quality assessment method for single-image super-resolution. In *2019 Chinese Control Conference (CCC)*, pages 3571–3576. IEEE.
- Yeganeh, H., Rostami, M., and Wang, Z. (2015). Objective quality assessment of interpolated natural images. *IEEE Transactions on Image Processing*, 24(11):4651–4663.
- Zhang, K., Zhu, D., Li, J., Gao, X., Gao, F., and Lu, J. (2021). Learning stacking regression for no-reference super-resolution image quality assessment. *Signal Processing*, 178:107771.
- Zhang, R., Isola, P., Efros, A. A., Shechtman, E., and Wang, O. (2018). The unreasonable effectiveness of deep features as a perceptual metric. In *Proceedings of the IEEE conference on computer vision and pattern recognition*, pages 586–595.
- Zhou, F., Yao, R., Liu, B., and Qiu, G. (2019). Visual quality assessment for super-resolved images: Database and method. *IEEE Transactions on Image Processing*, 28(7):3528–3541.
- Zhou, W., Wang, Z., and Chen, Z. (2021). Image super-resolution quality assessment: Structural fidelity versus statistical naturalness. *arXiv preprint arXiv:2105.07139*.